

SOME APPLICATIONS OF THE QUASI VORTEX-LATTICE METHOD
IN STEADY AND UNSTEADY AERODYNAMICS

C. Edward Lan
The University of Kansas

SUMMARY

The quasi vortex-lattice method is reviewed and applied to the evaluation of backwash, with applications in ground effect analysis. It is also extended to unsteady aerodynamics, with particular interest in the calculation of unsteady leading-edge suction. Some applications in ornithopter aerodynamics are given.

INTRODUCTION

The quasi vortex-lattice method (Quasi VLM) has been shown to produce good accuracy in lifting-surface problems not only for non-flapped but also flapped configurations (ref. 1). In these applications, the only induced velocity to be evaluated is the downwash. However, in some other applications such as ground effect analysis and wing-jet interaction (ref. 2), it is necessary to compute the u-induced velocity (i.e. backwash) in the flow field away from the wing plane. It is the purpose of this paper to assess the accuracy of such backwash computation.

One important feature of the Quasi VLM is the accurate prediction of the leading-edge suction without resorting to Kutta-Joukowski relation. It is this feature that makes it possible to extend the method to the prediction of unsteady leading-edge suction in unsteady aerodynamics. This extension is also presented below.

SYMBOLS

AR	aspect ratio
c	chord length, m(ft), taken as unity.
C	leading-edge singularity parameter, defined in eq. (3c)
$C_{D,i}$	induced drag coefficient
c_l	sectional lift coefficient
\bar{c}_l	amplitude of sectional lift coefficient in unsteady flow
C_L	total lift coefficient
C_{L_α}	lift curve slope, per radian
C_m	pitching moment coefficient
C_{m_α}	pitching moment curve slope, per radian
ΔC_p	pressure coefficient difference
\bar{C}_T	time-averaged leading-edge thrust coefficient
h, h_1	nondimensional height measured from the wing plane, referred to the chord length. See fig. 5.
\bar{h}	flapping amplitude
\bar{h}_t	flapping amplitude at the wing tip
k	reduced frequency, defined as $\omega c/2V$
M	number of integration points, or Mach number
N, N_c	number of chordwise vortices
N_s	number of spanwise vortex strips
S	leading-edge suction, $N(lb)$, or wing area, $m^2(ft^2)$

\bar{s}	amplitude of unsteady leading-edge suction
u	nondimensional backwash, positive downstream
\bar{u}	amplitude of unsteady backwash on the wing plane
V	freestream velocity, m/sec (ft/sec)
w	nondimensional downwash, positive downward
x, y, z	rectangular coordinates, with x positive downstream, y positive spanwise to the right and z positive upward
dz_c/dx	camber slope
α	angle of attack, deg.
$\bar{\alpha}$	amplitude of pitching oscillation
β	$= \sqrt{1-M^2}$
$\bar{\eta}$	propulsive efficiency, percent
η	nondimensional spanwise coordinate
γ	nondimensional vortex density
ω	oscillation frequency, rad/sec
ρ	density, kg/m ³ (slugs/ft ³)
q_∞	freestream dynamic pressure, N/m ² (lb/ft ²)
i	$= \sqrt{-1}$
$\bar{\delta}$	amplitude of flap angle
c_{l_∞}	sectional lift coefficient in free air

Subscript:

f flap

BASIC ANALYSIS IN QUASI VLM

For simplicity in presentation, consider the two-dimensional (2-D) downwash equation:

$$w(x) = \frac{1}{2\pi} \int_0^1 \frac{\gamma(x') dx'}{x-x'} \quad (1)$$

The integral is first transformed to a θ -integration and then reduced to a finite sum through the midpoint trapezoidal rule. It is obtained that

$$\begin{aligned} w(x_i) &= -\frac{1}{2\pi} \int_0^\pi \frac{\gamma(\theta') \sin\theta' d\theta'}{\cos\theta - \cos\theta'} = -\frac{1}{2\pi} \int_0^\pi \frac{\gamma' \sin\theta' - \gamma \sin\theta}{\cos\theta - \cos\theta'} d\theta' \\ &\approx -\frac{1}{2\pi} \frac{\pi}{N} \sum_{k=1}^N \frac{\gamma_k \sin\theta_k - \gamma_i \sin\theta_i}{\cos\theta_i - \cos\theta_k} \\ &= \frac{1}{4N} \sum_{k=1}^N \frac{\gamma_k \sin\theta_k}{x_i - x_k} + \begin{cases} NC, & i=0 \\ 0, & i \neq 0 \end{cases} \end{aligned} \quad (2)$$

where

$$x_i = \frac{1}{2} (1 - \cos\theta_i), \quad \theta_i = \frac{i\pi}{N}, \quad i = 0, 1, \dots, N \quad (3a)$$

$$x_k = \frac{1}{2} (1 - \cos\theta_k), \quad \theta_k = \frac{(2k-1)\pi}{2N}, \quad k = 1, \dots, N \quad (3b)$$

$$2C = \lim_{\theta \rightarrow 0} \gamma(\theta) \sin \theta \quad (3c)$$

Note that eq. (2) differs from the conventional VLM in that $\sin\theta$ in the formulation will eliminate the square-root singularities at the edges and the vortex densities are directly predicted, instead of the strengths of discrete vortices. Furthermore, the control and vortex points are defined by the so-called "semi-circle method." This is illustrated in fig. 1. By solving eq. (2) with $i \neq 0$, $N \gamma_k$ -values can be obtained. Then the leading-edge singularity parameter C can be computed by taking $i=0$, i.e., by taking control point at the leading edge. The leading-edge suction is then

$$S = \pi \rho \frac{C^2}{4} \quad (4)$$

In three-dimensional cases, the above concept is also applicable by treating each chordwise vortex integral in a similar manner as in eq. (2). In this case, not only chordwise control and vortex locations are defined by the semi-circle method, but also the spanwise vortex strips and control locations. See fig. 1. The detail is referred to in ref. 1. The rate of convergence of this method is indicated in figs. (2) and (3) for a 45°-sweep wing of AR=2 and constant chord. It is seen that the method converges reasonably fast.

BACKWASH EVALUATION AND GROUND EFFECT ANALYSIS

In ground effect analysis, it is known that the image vortex system may produce strong backwash to decrease the air velocity on the wing great enough to be significant. In fact, as a result the wing lift in ground effect may be less than the free air value. This unfavorable effect of backwash is particularly important in powered-lift aerodynamics and for wings under high lift conditions (ref. 3). Therefore, any formulation of ground-effect problem without backwash computation is applicable only to small loading conditions as analyzed in ref. 4.

To see the accuracy of backwash computation by VLM and Quasi VLM, consider the 2-D expressions for the backwash and downwash:

$$u(x, z) = \frac{z}{2\pi} \int_0^1 \frac{\gamma(x') dx'}{(x-x')^2 + z^2} \quad (5)$$

$$w(x, z) = \frac{1}{2\pi} \int_0^1 \frac{(x-x')\gamma(x') dx'}{(x-x')^2 + z^2} \quad (6)$$

If $\gamma(x') = \sqrt{(1-x')/x'}$, the integration can be performed exactly. The results are shown in Appendix A. The downwash expression is included here for later comparison. In all computations shown below, equal-spacing elements are used for the VLM. For the Quasi VLM, again the θ -transformation is applied first before using the midpoint trapezoidal rule. Fig. 4 shows that the backwash along the chord evaluated by the VLM at both control and vortex points tend to be too high, in particular near the leading edge. On the other hand, the Quasi VLM gives quite accurate results everywhere at these not too small z -values. With these results in mind, both methods are now applied to the following 2-D linear ground-effect equations:

$$\frac{1}{2\pi} \int_0^1 \frac{\gamma(x') dx'}{x-x'} - \frac{1}{2\pi} \int_0^1 \gamma(x') \frac{(x-x') - 2h_1\alpha}{(x-x')^2 + 4h_1^2} dx' = \alpha - \frac{dz}{dx} \quad (7)$$

$$c_l = 2 \int_0^1 \gamma(x)(1+u(x))dx \quad (8)$$

The corresponding geometry is given in fig. 5. The second integral in eq. (7) represents the normalwash due to the image vortex system. The "2h α " term is the backwash contribution. The results of computation are shown in fig. 6. Two points are of particular interest. Firstly, the linear vortex theory will give better results if the mean surface (as used in the mean surface approximation of the linear airfoil theory) is taken through the 3/4 chord point. Secondly, both the Quasi VLM and VLM predict approximately the same lift, despite the fact that the VLM gives higher backwash. This is because the VLM also produces higher downwash at a given z-value. This is shown in fig. 7. This means that the higher upwash from the image vortex system as predicted by the VLM tends to compensate the effect due to the higher predicted backwash. With flap deflected, the VLM predicts lower lift than the Quasi VLM does as shown in fig. 8.

The analysis with eqs. (7)-(8) becomes increasingly inaccurate at $h < 0.2$. As an extreme example, let $z=0.05$ in eq. (5). With $\gamma = \sqrt{(1-x)/x}$, the results are shown in figs. 9 and 10. It is seen that the backwash is underpredicted at the control points and overpredicted at the vortex points by both the VLM and the Quasi VLM. Depending on α , this would result in small or even negative c_l in eq. (8). The backwash computation with small z has important applications in wing-jet interaction theory (ref. 2). Therefore, it is desirable to find a practical way to improve the accuracy of the computation. Even though increasing the number of vortex points (i.e. the number of integration points) can increase the accuracy, it is not a practical way because the number of unknowns to be solved would greatly increase, in particular, in 3-D applications. Since the inaccuracy is mainly due to the second-order singularity in eq. (5) as $z \rightarrow 0$, a practical method is described in ref. 6 to deal with this by weakening the singularity. According to this method, eq. (5) is evaluated as follows:

$$u(x,z) = \frac{z}{2\pi} \int_0^1 \frac{\gamma(x') - \gamma(x)}{(x-x')^2 + z^2} dx' + \frac{z\gamma(x)}{2\pi} \int_0^1 \frac{dx'}{(x-x')^2 + z^2} \quad (9)$$

$$\approx \frac{z}{4\pi} \frac{\pi}{N} \sum_{k=1}^N \frac{[\gamma(x_k) - \gamma(x)]_k}{(x-x_k)^2 + z^2} \cdot \sin\theta_k + \frac{z\gamma(x)}{4\pi} \frac{\pi}{M} \sum_{j=1}^M \frac{\sin\theta_j}{(x-x_j)^2 + z^2} \quad (10)$$

where x may be the control points (eq. 3a) or the vortex locations (eq. 3b) and

$$x_j = \frac{1}{2} (1 - \cos\theta_j), \quad \theta_j = \frac{(2j-1)\pi}{2M}, \quad j=1, \dots, M \quad (11)$$

with M chosen to be $2^p N$ for interdigitation between control and vortex points, p being any integer. Note that the last integral in eq. (9) can be integrated exactly in 2-D case. However, the similar integral in 3-D would be too complicated to integrate. The accuracy of eq. (10) is also demonstrated with $p=3$ in figs. 9-10. Its application in a wing-jet interaction theory is discussed in ref. 7.

PREDICTION OF UNSTEADY LEADING-EDGE SUCTION

As mentioned earlier, the Quasi VLM predicts the leading-edge suction through the computation of the leading-edge singularity parameter. This feature can be easily extended to the unsteady aerodynamics if the downwash expression similar to that due to a steady horseshoe vortex can be derived for unsteady flow. This has been done recently by integrating the doublet potential by parts. The results are given in Appendix B for planar configurations. Note that if the oscillating frequency is zero, the expression is reduced to that for a steady horseshoe vortex. Using this expression, it is possible to extend the steady Quasi VLM to the unsteady case. In 2-D flow, this has been done in ref. 8. Some comparison with exact solutions of unsteady leading-edge suction (ref. 9) is made in Table I. It is seen that the accuracy of the Quasi VLM is quite good. Other aerodynamic characteristics at low or high subsonic Mach numbers can also be predicted accurately, including gust response (ref. 8).

In the 3-D method, note that the downwash expression given in Appendix B involves two types of integrals. The integration associated with I-integral, eqs. (B.15) and (B.18), can be performed by approximating the integrand, as has been done in ref. 10. On the other hand, the integrals, F_2 and F_4 , can most conveniently be integrated by approximating the integrands by quadratic functions of the integration variable as has been done in ref. 10. The remaining aspects of the method follow closely the steady version.

To show the 3-D applications, the characteristics of a rectangular wing of aspect ratio 2 undergoing the first bending mode of oscillation (ref. 11) are computed. To indicate the rate of convergence of the method, the predicted complex lift coefficient is plotted in fig. 11 against the number of spanwise strips. It is seen that the method converges relatively fast for this planform. For instance, with $N_c=4$, C_L is changed by only 1% as N_s is increased from 10 to 20. Furthermore, the effect of N_c is seen to be small for this wing without chordwise deformation. The predicted pressure distributions at one spanwise station are compared with experimental data and those predicted by the Doublet-Lattice Method (DLM) (ref. 10) in fig. 12 with good agreement. The 3-D exact solution of unsteady leading-edge suction is not available. However, Bennett (ref. 12) has applied Reissner's high aspect-ratio theory to the computation of propulsive efficiency of ornithopters.

Here, the propulsive efficiency is defined as

$$\bar{\eta} = \frac{q_{\infty} S \bar{C}_T V}{q_{\infty} S C_L \dot{h}} \quad (12)$$

$$\bar{C}_L \dot{h} = \frac{1}{2} \omega \int_{-1}^1 \bar{h}(\eta) \bar{c}_l(\eta) d\eta \quad (13)$$

All quantities in eq. (12) have been averaged over one cycle. The results for two rectangular wings of aspect ratios of 6 and 12 performing linear flapping ($\bar{h}(\eta) = \bar{h}_t \eta$) are shown in fig. 13. It appears that the high aspect ratio theory tends to predict higher thrust than the present method. The agreement of the predicted efficiency by both methods is good for AR=12. But for AR=6, the high aspect-ratio theory predicts lower efficiency, presumably because it would predict much higher input power which depends on the wing loading.

CONCLUDING REMARKS

The quasi vortex-lattice method was shown to possess good convergence characteristics in steady wing theory. Its application to the computation of downwash and backwash away from the wing plane in 2-D flow showed better accuracy than the conventional VLM with z not too small. When z is small, both methods become inaccurate in backwash computation. An improved method for the Quasi VLM was presented. The Quasi VLM was also extended to the unsteady aerodynamics, with the calculation of unsteady leading-edge suction being of particular interest.

APPENDIX A

Exact Integration for Eqs. (5) and (6)

(1) Eq. (5)

$$u(x,z) = \frac{z}{2\pi} \int_0^1 \frac{\sqrt{\frac{1-x'}{x'}}}{(x-x')^2+z^2} dx' = \frac{az}{2\pi} \frac{b(1-x)-a^2}{a^4+b^2z^2} \left\{ \frac{\pi}{2} \text{sign}[b(1-x)-a^2] \right. \\ \left. + \frac{\pi}{2} \text{sign}[bx+a^2] \right\} \quad (\text{A.1})$$

where

$$b = \frac{1}{2}(1-2x) \quad (\text{A.2})$$

$$a^2 = \frac{\sqrt{[z^2+x(1-x)]^2+(1-2x)^2z^2} - [z^2+x(1-x)]}{2} \quad (\text{A.3})$$

(2) Eq. (6)

$$w(x,z) = \frac{1}{2\pi} \int_0^1 \frac{(x-x')\sqrt{\frac{1-x'}{x'}}}{(x-x')^2+z^2} dx' = \frac{(D-D^{-1})\cos\theta_1 + D^2 - \cos 2\theta_1}{D^2 + D^{-2} - 2\cos 2\theta_1}$$

where

$$D = \sqrt{2} / \left\{ [2+Z'+(Z'^2+16z^2)^{\frac{1}{2}}]^{\frac{1}{2}} + [Z'+(Z'^2+16z^2)^{\frac{1}{2}}]^{\frac{1}{2}} \right\} \quad (\text{A.4})$$

$$\theta_1 = \cos^{-1} \left\{ \left[\frac{2}{2+Z' + (Z'^2+16z^2)^{\frac{1}{2}}} \right]^{\frac{1}{2}} \cos\theta \right\} \quad (\text{A.5})$$

$$Z' = 4z^2 - \sin^2\theta \quad (\text{A.6})$$

$$\cos\theta = 1-2x \quad (\text{A.7})$$

APPENDIX B

Downwash due to an Oscillating Horseshoe Vortex

The downwash produced by an "oscillating horseshoe vortex" for a planar configuration can be written as

$$\frac{\partial \phi}{\partial z} = \frac{\partial \phi_1}{\partial z} + \frac{\partial \phi_2}{\partial z} \quad (\text{B.1})$$

where

$$\frac{\partial \phi_1}{\partial z} = F_1 + F_2 \quad (\text{B.2})$$

$$\frac{\partial \phi_2}{\partial z} = F_3 + F_4 \quad (\text{B.3})$$

$$F_1 = \frac{\Delta C_P}{8\pi} \left\{ -\frac{1}{y'-y} + \frac{1}{\sqrt{(x-x')^2 + \beta^2(y-y')^2}} \right. \\ \times \left[\frac{x'-x}{y'-y} + \frac{(x'-x)(x_2-x_1) + \beta^2(y_2-y_1)(y'-y)}{Q} \right] \left. \right\} \\ \times \exp \left\{ -i\frac{\omega}{V} \frac{M \sqrt{(x-x')^2 + \beta^2(y-y')^2} - M^2(x-x')}{\beta^2} \right\} \begin{cases} x'=x_2 \\ y'=y_2 \\ x'=x_1 \\ y'=y_1 \end{cases} \quad (\text{B.4})$$

$$\begin{aligned}
F_2 = & -i\frac{\omega}{V} \frac{\Delta C_P}{8\pi} \int_0^1 \left\{ -\frac{1}{\eta-y} + \frac{1}{(y_2-y_1)R} \left[\frac{(x_2-x_1)(\eta-y)+Q}{\eta-y} \right. \right. \\
& \left. \left. + \frac{((x_2-x_1)(\eta-y)+Q)(x_2-x_1) + \beta^2(y_2-y_1)^2(\eta-y)}{Q} \right] \right\} \\
& \times \left[\frac{M(\eta-y)}{R} + \left(\frac{M}{\beta^2} \frac{x_0}{R} - \frac{M^2}{\beta^2} \frac{x_2-x_1}{y_2-y_1} \right) \exp \left[-i\frac{\omega}{V} \frac{MR-M^2x_0}{\beta^2} \right] (y_2-y_1) \right] d\tau \quad (B.5)
\end{aligned}$$

$$R = \sqrt{A\tau^2 + B\tau + C} \quad (B.6)$$

$$A = (x_2-x_1)^2 + \beta^2(y_2-y_1)^2 \quad (B.7)$$

$$B = -2[(x-x_1)(x_2-x_1) + \beta^2(y-y_1)(y_2-y_1)] \quad (B.8)$$

$$C = (x-x_1)^2 + \beta^2(y-y_1)^2 \quad (B.9)$$

$$\eta-y = (y_2-y_1)\tau - (y-y_1) \quad (B.10)$$

$$Q = (x_2-x_1)(y-y_1) - (x-x_1)(y_2-y_1) \quad (B.11)$$

$$x_0 = x-x_1 - \tau(x_2-x_1) \quad (B.12)$$

$$F_3 = -i\frac{\omega}{V} \frac{\Delta C_P}{8\pi} \left\{ -\frac{1}{y_2-y} I_2 + \frac{1}{y_1-y} I_1 \right\} \quad (B.13)$$

$$F_4 = -i\frac{\omega}{V} \frac{\Delta C_P}{8\pi} \int_0^1 \frac{1}{\eta-y} \frac{\partial I}{\partial \eta} (y_2-y_1) d\tau \quad (B.14)$$

$$I(\tau) = \int_{\tau_1 r_1}^{\infty} \left(1 - \frac{\tau'}{\sqrt{\tau'^2 + r_1^2}}\right) e^{-i\frac{\omega}{V}(\tau' + x_0)} d\tau' \quad (\text{B.15})$$

$$\tau_1 r_1 = \frac{-x_0 + MR}{\beta^2} \quad (\text{B.16})$$

$$r_1^2 = (y - \eta)^2 \quad (\text{B.17})$$

$$(\tau_1 r_1)_1 = \tau_1 r_1 \text{ at } \tau=0$$

$$(\tau_1 r_1)_2 = \tau_1 r_1 \text{ at } \tau=1$$

$$r_{11}^2 = r_1^2 \text{ at } \tau=0$$

$$r_{12}^2 = r_1^2 \text{ at } \tau=1$$

$$x_{01} = x_0 \text{ at } \tau=0$$

$$x_{02} = x_0 \text{ at } \tau=1$$

$$\begin{aligned} \frac{\partial I}{\partial \eta} &= \frac{M(y-\eta)}{R} \left(1 - \frac{\tau_1}{\sqrt{1+\tau_1^2}}\right) e^{-i\frac{\omega}{V}(\tau_1 r_1 + x_0)} + i\frac{\omega}{V} I(\tau) \frac{x_2 - x_1}{y_2 - y_1} \\ &+ \left(1 - \frac{\tau_1}{\sqrt{1+\tau_1^2}}\right) e^{-i\frac{\omega}{V}(\tau_1 r_1 + x_0)} \left(\frac{Mx_0}{\beta^2 R} - \frac{1}{\beta^2}\right) \frac{x_2 - x_1}{y_2 - y_1} \\ &- (y - \tau_1) \int_{\tau_1 r_1}^{\infty} \frac{\tau'}{(\tau'^2 + r_1^2)^{3/2}} e^{-i\frac{\omega}{V}(\tau' + x_0)} d\tau' \end{aligned} \quad (\text{B.18})$$

In the above expressions, (x_1, y_1) and (x_2, y_2) represent inboard and outboard endpoints of the "bounded element," respectively.

REFERENCES

1. Lan, C. Edward: A Quasi Vortex-Lattice Method in Thin Wing Theory. *Journal of Aircraft*, Vol. 11, No. 9, Sept. 1974, pp. 518-527.
2. Lan, C. Edward and Campbell, James F.: Theoretical Aerodynamics of Upper-Surface-Blowing Jet-Wing Interaction. NASA TN D-7936, 1975.
3. Gratzler, L.B. and Mahal, A.S.: Ground Effects in STOL Operation. *Journal of Aircraft*, Vol. 9, No. 3, March 1972, pp. 236-242.
4. Saunders, G.H.: Aerodynamic Characteristics of Wings in Ground Proximity. *Canadian Aeronautics and Space Journal*, Vol. 11, No. 6, June 1965, pp. 185-192.
5. Thwaites, B.: *Incompressible Aerodynamics*. Oxford-Clarendon Press, 1960.
6. Lan, C. Edward: An Analytical Investigation of Wing-Jet Interaction. Section 6. NASA CR-138140, April 1974.
7. Lan, C. Edward: Upper-Surface-Blowing Jet-Wing Interaction. Vortex-Lattice Utilization, NASA SP-405, 1976. (Paper no. 11 of this compilation.)
8. Lan, C. Edward: The Induced Drag of Oscillating Airfoils in Linear Subsonic Compressible Flow. KU-FRL-400, June 1975, The Flight Research Laboratory, The University of Kansas Center for Research, Inc.
9. Garrick, I. E.: Propulsion of a Flapping and Oscillating Airfoil. NACA Report No. 567, 1936.
10. Albano, Edward and Rodden, William P.: A Doublet-Lattice Method for Calculating Lift Distributions on Oscillating Surfaces in Subsonic Flows. *AIAA Journal*, Vol. 7, No. 2, Feb. 1969. pp. 279-285.
11. Lessing, H.C.; Troutman, J.L.; and Menees, G.P.: Experimental Determination of the Pressure Distribution on a Rectangular Wing Oscillating in the First Bending Mode for Mach Numbers from 0.24 to 1.30. NASA TN D-344, 1960.
12. Bennett, Albert George, Jr.: A Preliminary Study of Ornithopter Aerodynamics. Ph.D. dissertation, 1970. University of Illinois.

Table I. -- Comparison of Predicted Leading-Edge Suction Parameter with Exact Solutions in 2-D Incompressible Flow.

$$\bar{s} = \lim_{x \rightarrow -1} \bar{u}(x) \sqrt{1+x}$$

$$\bar{s}_\alpha = \partial \bar{s} / \partial \alpha, \quad \bar{s}_\delta = \partial \bar{s} / \partial \delta$$

(A) Pitching motion about midchord

\underline{k}	\underline{N}	<u>Present Method</u>	\bar{s}_α	<u>Exact, Ref. 9</u>
0.1	10	1.18870-0.25555i		1.18870-0.25556i
0.5	15	0.89889-0.35527i		0.89889-0.35529i
1.0	15	0.83374-0.46737i		0.83378-0.46748i

(B) Flap Rotation with flap-chord ratio = 0.3

\underline{k}	$(\underline{N}_1, \underline{N}_2)$	<u>Present Method</u>	\bar{s}_δ	<u>Exact, Ref. 9</u>
0.1	(12, 7)	0.37115-0.14696i		0.37139-0.14705i
0.5	(12, 7)	0.17483-0.11565i		0.17496-0.11576i
1.0	(12, 7)	0.12972-0.06580i		0.12982-0.06592i

Note: N_1 = number of doublet elements on the airfoil.
 N_2 = number of doublet elements on the flap.

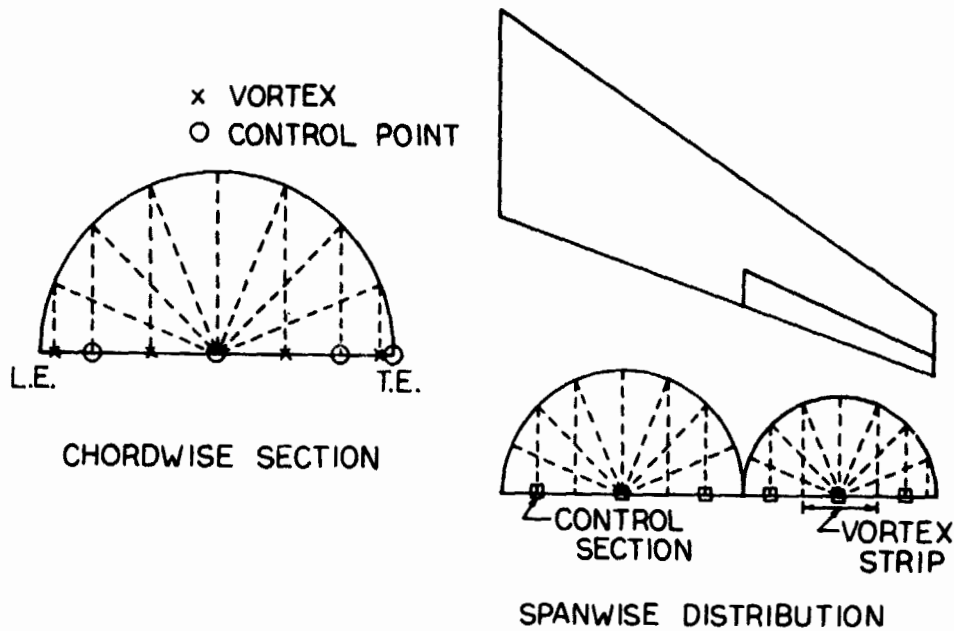


Figure 1.- Illustration of chordwise and spanwise control and vortex locations.

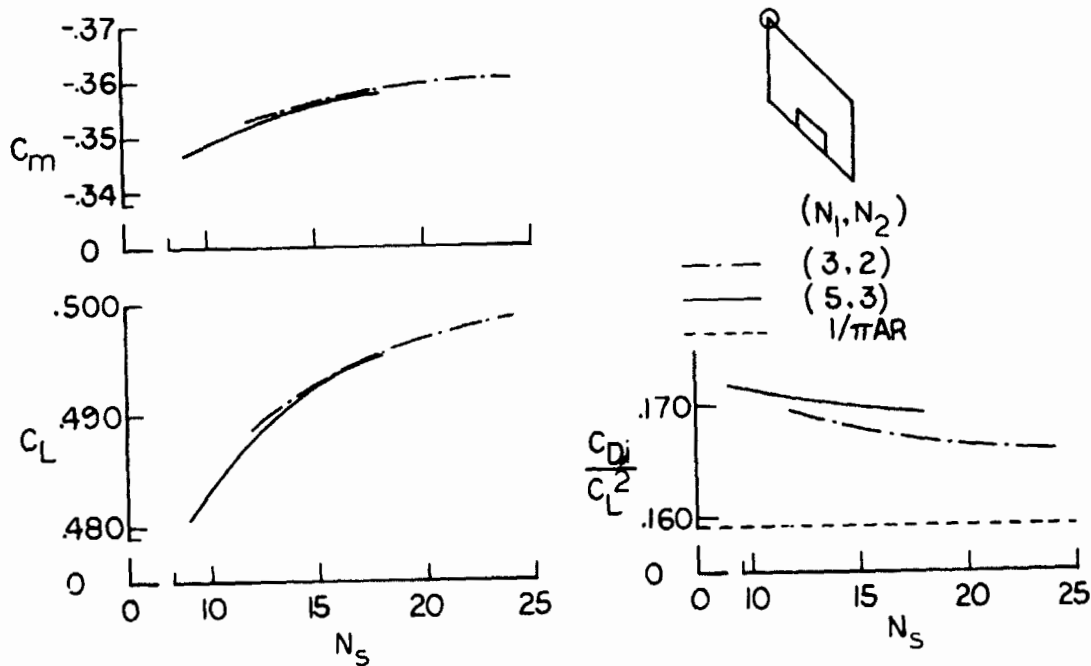


Figure 2.- Effect of vortex-lattice arrangement on aerodynamic characteristics of a 45° -sweep wing of $AR = 2$. $\delta_f = 0^\circ$; $M = 0$.

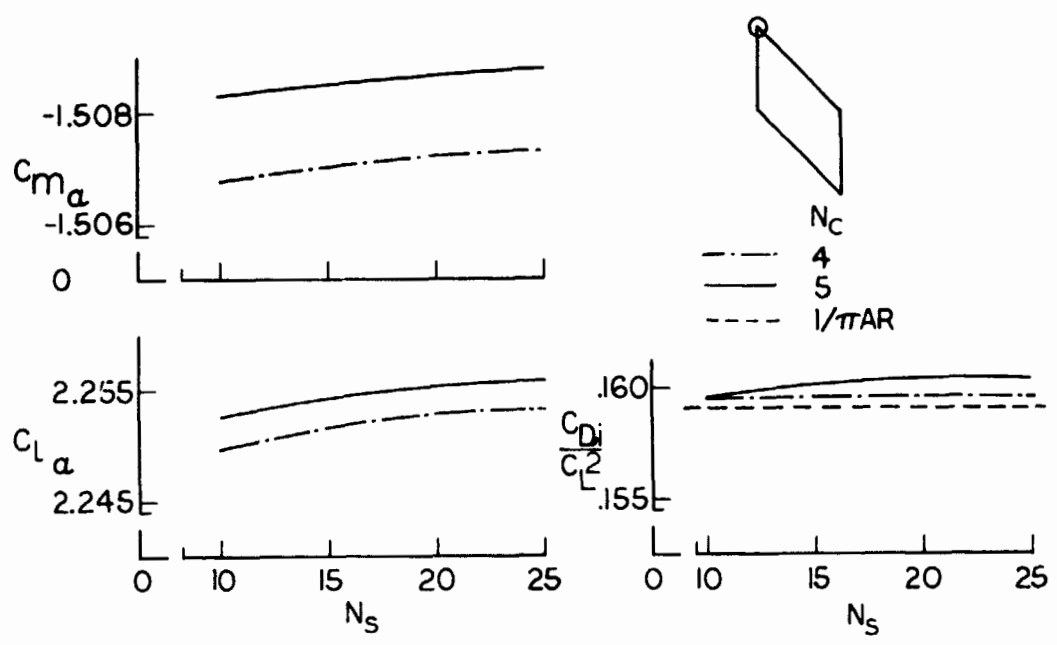
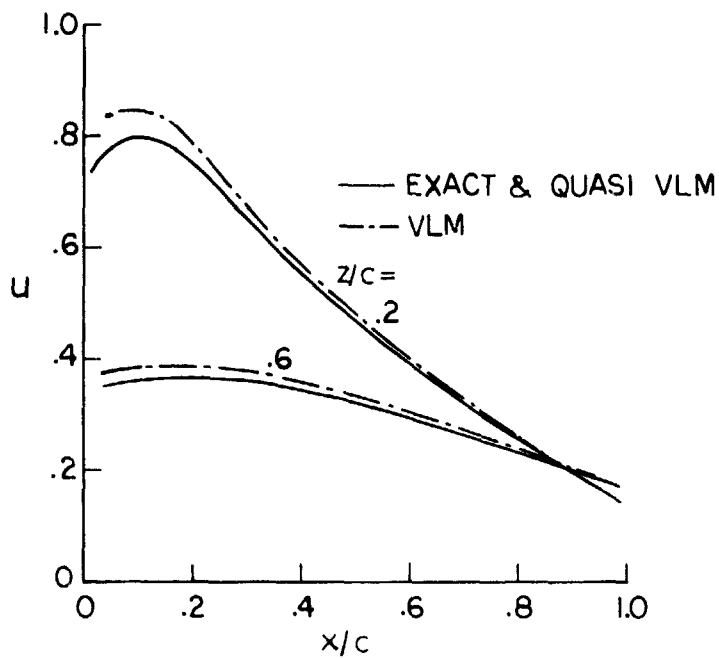
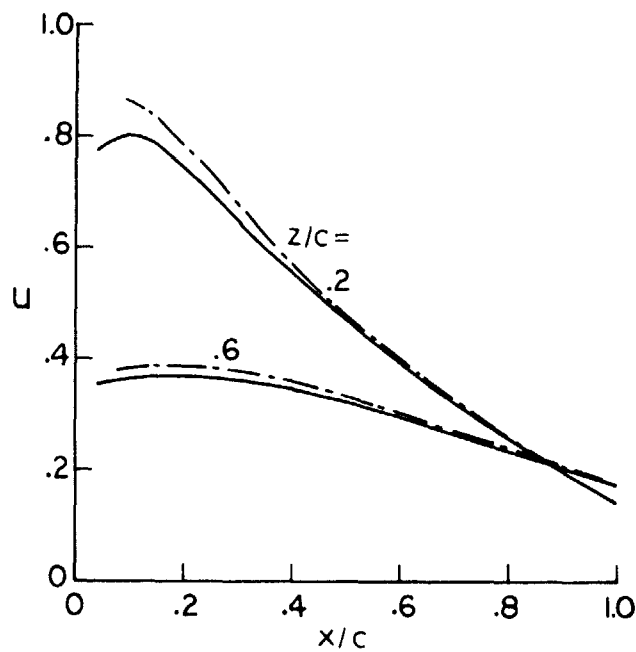


Figure 3.- Effect of vortex-lattice arrangement on aerodynamic characteristics of a 45°-sweep wing of AR = 2. $\delta_f = 10^\circ$; $\alpha = 10^\circ$; and M = 0.5.



(a) At vortex points.



(b) At control points.

Figure 4.- Comparison of backwash evaluations (eq. 5) by different methods. $\gamma(x) = \sqrt{(1-x)/x}$; $N = 8$.

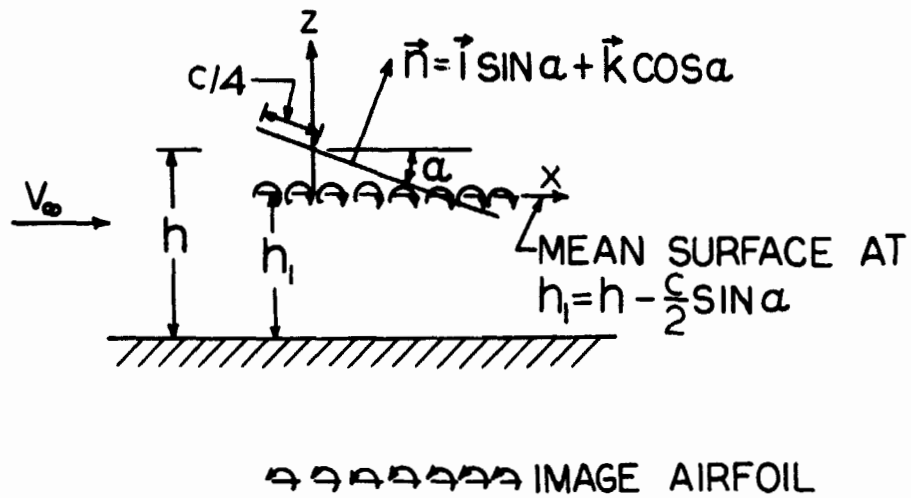


Figure 5.- Geometry for the ground-effect equation.

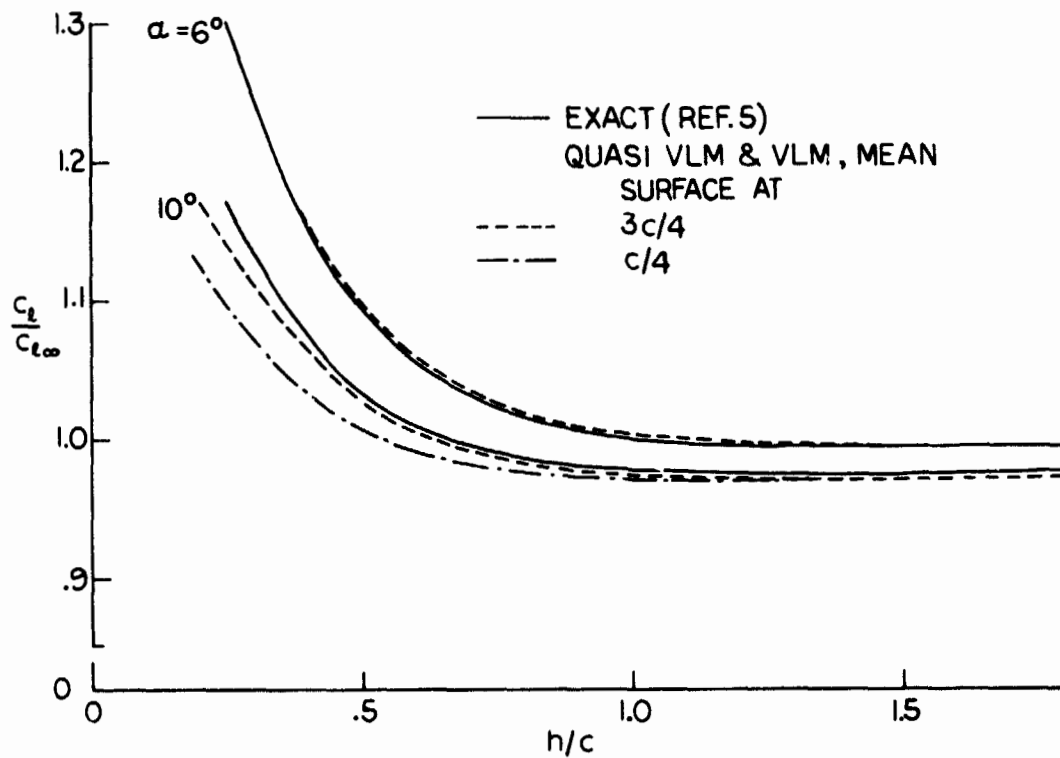


Figure 6.- Comparison of computed airfoil lift in ground effect by different methods. $c_{l_\infty} = 2\pi\alpha$; h measured from c/4.

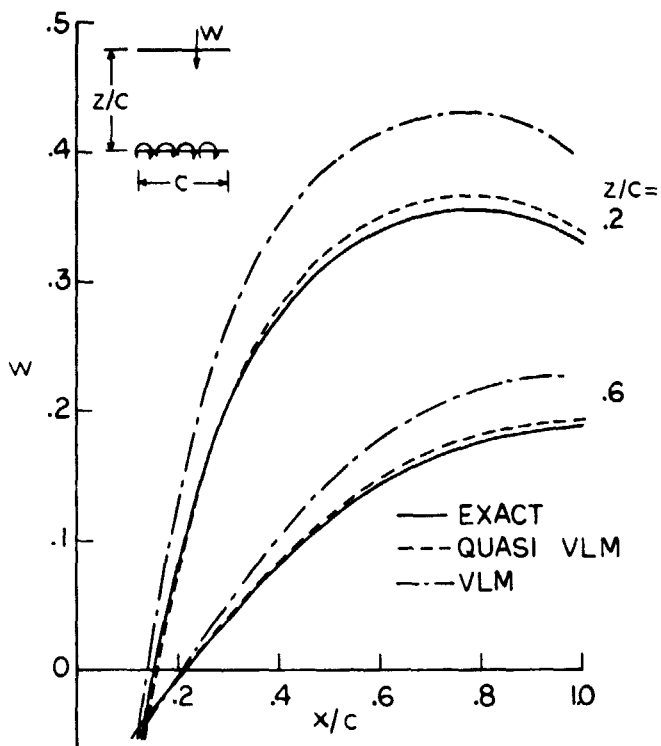


Figure 7.- Comparison of downwash evaluations (eq. 6) at control points by different methods. $\gamma(x) = \sqrt{(1-x)/x}$; $N = 8$.

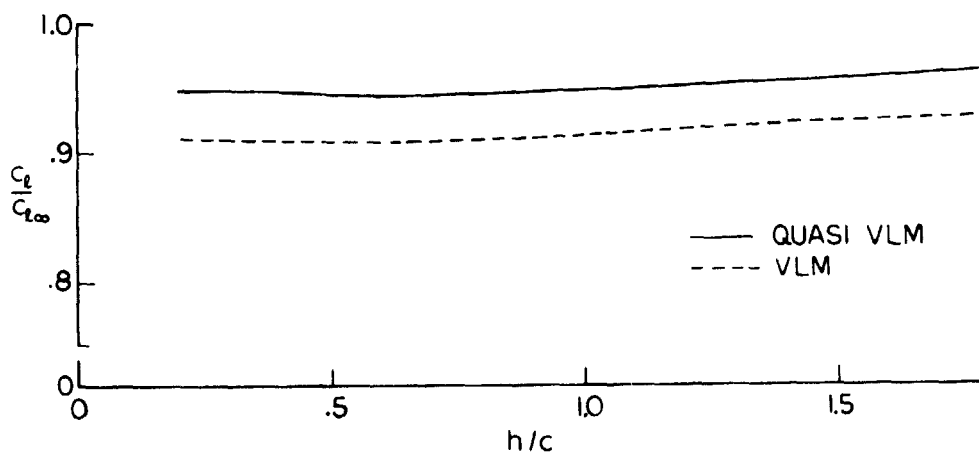


Figure 8.- Comparison of computed airfoil lift in ground effect by different methods. $c_f/c = 0.3$; $\delta_f = 20^\circ$; $\alpha = 2^\circ$; $c_{l_\infty} = 1.6685$; h measured from $c/4$.

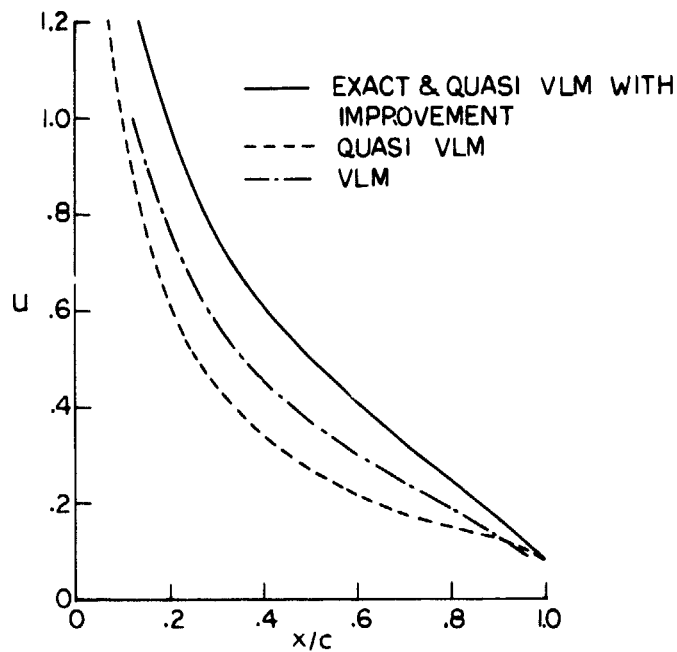


Figure 9.- Comparison of backwash evaluations at control points by different methods. $\gamma(x) = \sqrt{(1-x)/x}$; $z/c = 0.05$; $N = 6$.

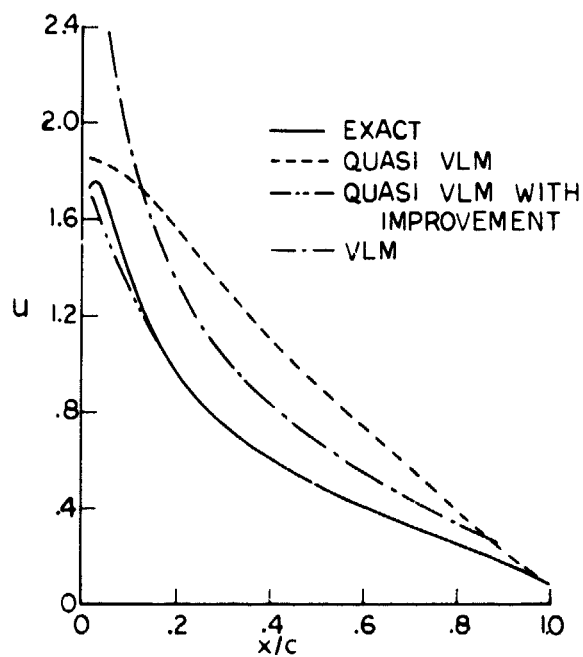


Figure 10.- Comparison of backwash evaluations at vortex points by different methods. $\gamma(x) = \sqrt{(1-x)/x}$; $z/c = 0.05$; $N = 6$.

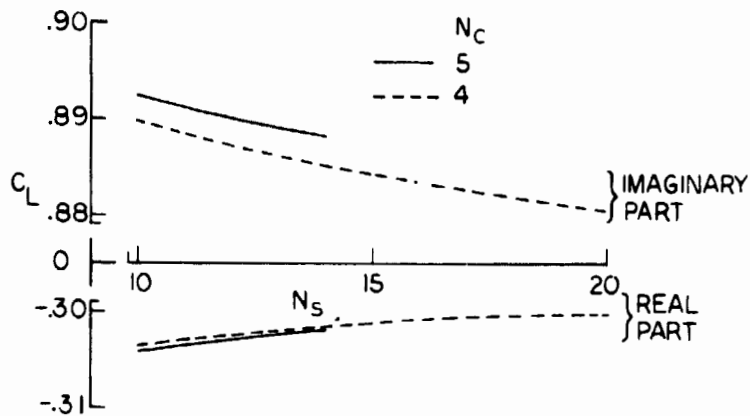


Figure 11.- Convergence of computed lift coefficient for a rectangular wing of AR = 2 oscillating in first bending mode. $M = 0.24$; $k = 0.47$.

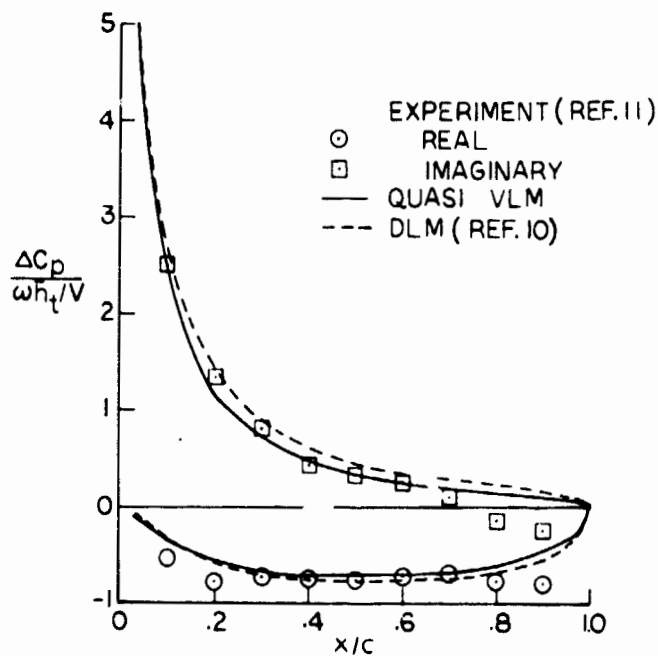
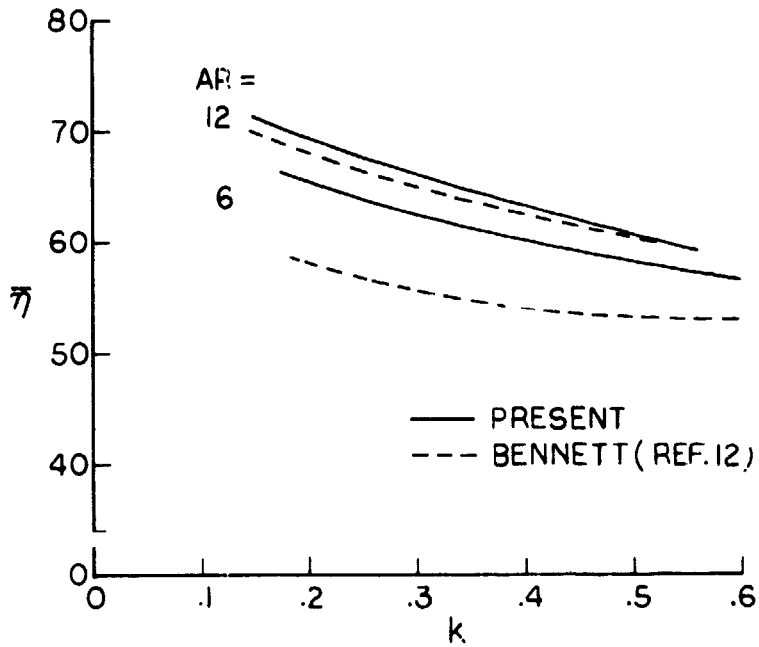
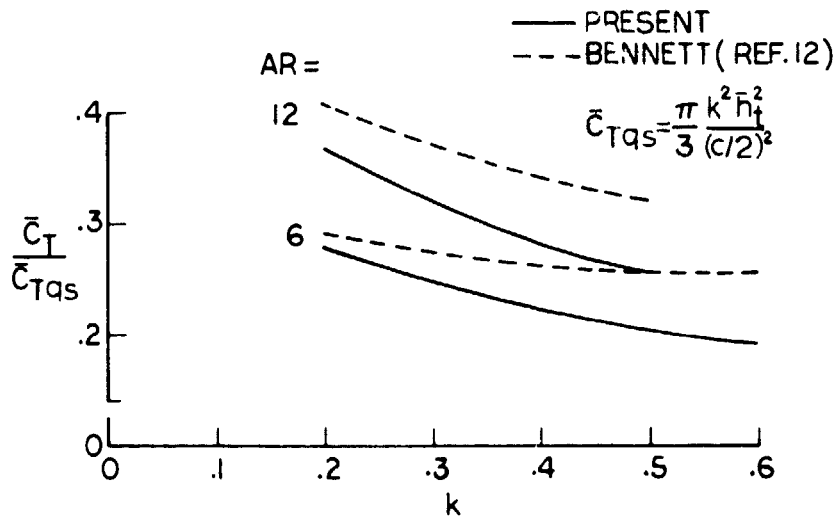


Figure 12.- Comparison of computed pressure distributions with experimental data for a rectangular wing of AR = 2 oscillating in first bending mode. $M = 0.24$; $k = 0.47$.



(a) Propulsive efficiency.



(b) Thrust.

Figure 13.- Theoretical propulsive efficiency and thrust for rectangular wings in linear flapping.